Published in final edited form as:
Invest Ophthalmol Vis Sci. 2009 December ; 50(12): 5778–5784. doi:10.1167/iovs.09-3790.

Automated Segmentation of the Cup and Rim from Spectral Domain OCT of the Optic Nerve Head

Michael D. Abràmoff[1,2,3], **Kyungmoo Lee**[3,4], **Meindert Niemeijer**[1,3], **Wallace L. M. Alward**[1], **Emily C. Greenlee**[1,2], **Mona K. Garvin**[3], **Milan Sonka**[1,3], and **Young H. Kwon**[1]

[1]Department of Ophthalmology and Visual Sciences, University of Iowa Hospitals and Clinics, Iowa City, Iowa

[2]Department of Veterans Affairs, Iowa City VA Medical Center, Iowa City, Iowa

[3]Department of Electrical and Computer Engineering, University of Iowa, Iowa City, Iowa

[4]Department of Biomedical Engineering, University of Iowa, Iowa City, Iowa

Abstract

PURPOSE—To evaluate the performance of an automated algorithm for determination of the cup and rim from close-to-isotropic spectral domain (SD) OCT images of the optic nerve head (ONH) and compare to the cup and rim as determined by glaucoma experts from stereo color photographs of the same eye.

METHODS—Thirty-four consecutive patients with glaucoma were included in the study, and the ONH in the left eye was imaged with SD-OCT and stereo color photography on the same day. The cup and rim were segmented in all ONH OCT volumes by a novel voxel column classification algorithm, and linear cup-to-disc (c/d) ratio was determined. Three fellowship-trained glaucoma specialists performed planimetry on the stereo color photographs, and c/d was also determined. The primary outcome measure was the correlation between algorithm-determined c/d and planimetry-derived c/d.

RESULTS—The correlation of algorithm c/d to experts 1, 2, and 3 was 0.90, 0.87, and 0.93, respectively. The c/d correlation of expert 1 to 2, 1 to 3, and 2 to 3, were 0.89, 0.93, and 0.88, respectively.

CONCLUSIONS—In this preliminary study, we have developed a novel algorithm to determine the cup and rim in close-to-isotropic SD-OCT images of the ONH and have shown that its performance for determination of the cup and rim from SD-OCT images is similar to that of planimetry by glaucoma experts. Validation on a larger glaucoma sample as well as normal controls is warranted.

Glaucoma is the second leading cause of blindness in the United States, characterized by gradual damage to the optic nerve and resultant visual field loss.1 Early diagnosis and optimal treatment have been shown to minimize the risk of visual loss due to glaucoma.[2] The hallmark of glaucoma is cupping of the optic disc, which is the visible manifestation of a three-dimensional structure, the optic nerve head (ONH), in two dimensions. The optic disc can be imaged two dimensionally, either through indirect stereo biomicroscopy or with stereo color

Corresponding author: Michael D. Abràmoff, Department of Ophthalmology and Visual Sciences, University of Iowa Hospitals and Clinics, 200 Hawkins Drive, Iowa City, IA 52242; michael-abramoff@uiowa.edu.

Disclosure: **M.D. Abràmoff**, Carl Zeiss Meditec, Inc. (F), P; **Y.H. Kwon**, P; **M. Sonka**, Carl Zeiss Meditec, Inc. (F), P; **M. Garvin**, Carl Zeiss Meditec, Inc. (F), P

fundus photography. The ratio of the optic disc cup and neuroretinal rim surfaces, or cup-to-disc (c/d) ratio, is an important structural indicator for assessing the presence and progression of glaucoma. To quantify the ratio, planimetry has been performed by glaucoma specialists from stereo color photographs of the optic disc.[3,4] However, it has been shown that manual planimetry is time-consuming with substantial interobserver variability.5 We and others have previously presented and validated algorithms to segment the cup and the rim of the optic disc from stereo color photographs.[6–9] We used pixel feature classification, a machine learning technique, to assign a label to the pixels in color stereo images of the optic disc as cup, rim, or background, and were able to determine the c/d ratio with a performance comparable to that of glaucoma fellows in a small group of patients with glaucoma.[6]

With the introduction of spectral-domain optical coherence tomography (SD-OCT),[10,11] imaging of the three-dimensional structure of the ONH is now possible. Some commercially available scanners are capable of acquiring close-to-isotropic 3-D ONH-centered volumes. *Isotropic* means that the size of each imaged element, or voxel, is the same in all three dimensions. Another way of explaining isotropism is that the spacing between the acquired B-scans (in what we call the *y*-dimension) is the same as the distance between each A-scan within that B-scan (in what we call the *x*-dimension). Available SD-OCT scanners are never truly isotropic, because the retinal tissue in each A-scan is sampled at smaller differences in depth than the distance between A and/or B-scans—the resolution in the depth (or what is called the *z*-dimension) is always higher than the resolution in the *x*- and *y*-dimensions. The primary advantage of more isotropic imaging in quantifying properties of the ONH is that fewer assumptions have to be made about the tissue between measured samples, potentially leading to more accurate ONH metrics.

Direct quantification of optic nerve head parameters from close-to-isotropic SD-OCT images has the potential to improve the management of patients with glaucoma. However, clinical management of such patients is historically based on assessment of the *optic disc* as discussed earlier,[12] as well as other parameters. Specific properties of the visible disc, including subtle color changes, which may be helpful to the clinician, are lost in (narrow-band) SD-OCT.

Because glaucoma is a slowly progressing disease, with changes occurring over many years, it is currently not clear which ONH parameters, as derived from SD-OCT, if any, are suitable for measurement of glaucoma progression. SD-OCT may be used to quantify glaucoma and glaucoma progression in new ways, as exemplified by the work of Burgoyne et al.[13–15] Until such new metrics are validated clinically, however, the segmentation of the optic nerve head into neuroretinal rim and cup by SD-OCT may be helpful in making comparisons with historically accepted optic disc planimetry data, as well as to facilitate interpretation by clinicians.

Typically, before the advent of SD-OCT, up to six B-scans or OCT slices were obtained from the optic nerve head during each scanning session, and these were evaluated visually by the individual clinician. With SD-OCT, visual evaluation of all imaging data has become impossible because substantially more data are acquired. The SD-OCT images used in this work contained 200 × 200 × 1024 voxels, which is 52 times the number of voxels in a typical time-domain sequence with 6 × 128 × 1024 voxels, illustrating the need for automated techniques to analyze these datasets.

We extended our pixel classification approach to use SD-OCT-derived features to segment SD-OCT optic nerve head images, and the purpose of this preliminary study was to determine the performance of the algorithm's cup–rim segmentation from SD-OCT images to planimetry by glaucoma experts in patients with glaucoma or suspicion of glaucoma.[5]

METHODS

Subject Selection

SD-OCT images of the optic nerve head and fixed-base color stereo photographs of the optic disc, from both eyes, were obtained on the same day from 34 consecutive patients from the Glaucoma Clinic at the University of Iowa, according to inclusion criteria and a protocol that will be described later. The study was approved by our Institutional Review Board and adhered to the tenets of the Declaration of Helsinki; written informed consent was obtained. As in our previous work, patients with glaucoma were included if they met the definition of suspected glaucoma, open-angle glaucoma, angle-closure glaucoma, or combined-mechanism glaucoma. Any nonglaucomatous optic neuropathy was excluded. The diagnosis of suspected glaucoma was based on suspicious optic nerve appearance (enlarged cupping on clinical examination) with normal visual field and intraocular pressure (IOP) ≤ 21 mm Hg; it also included those with normal optic disc appearance on biomicroscopy and normal visual field, but with elevated IOP (> 21 mm Hg). The open-angle glaucoma diagnosis included patients with both primary and secondary open-angle glaucoma and was based on the presence of an open iridocorneal angle, glaucomatous optic disc and/or nerve fiber layer defects on biomicroscopy, and visual field changes (regardless of IOP level). Glaucomatous optic discs were identified as those with either diffuse or focal thinning of the neuroretinal rim. Visual field abnormalities were considered to be glaucomatous if they were consistent with the optic nerve examination and had either a typical nerve fiber layer distribution, or glaucoma hemifield test results outside normal limits. Angle-closure glaucoma included primary and secondary angle closure and narrow or appositionally closed, occludable angles. However, acute angle-closure glaucoma was excluded. The optic disc and visual field criteria for glaucoma were the same as those for open-angle glaucoma. Finally, combined-mechanism glaucoma included cases that had both open- and closed-angle components. The optic disc and visual field criteria were the same as for open-angle glaucoma. The diagnoses were made by the treating glaucoma specialist according to these definitions.

Data Collection

SD-OCT scans were acquired (Cirrus; Carl Zeiss Meditec, Inc., Dublin, CA) with an OCT scanner, in the 200 × 200 × 1024 mode. OCT scans were exported in uncompressed raw format (40 Mb per scan), preserving the voxel intensities.

Color slide stereo photographs centered on the optic disc of both eyes were acquired using a fixed stereo-base stereo retinal camera (3Dx; Nidek, Newark, NJ), with a digital back. The left and right stereo images of the selected stereo pairs were downsampled to 768 × 1019 pixels, by automatically locating the optic discs in the left and right parts of these 3072 × 2048 images.[16] The cropped images included the optic disc in its entirety in all images.

Computer-aided planimetry of the stereo pairs with a hand-held stereoscope was performed by three faculty glaucoma specialists at the University of Iowa on the stereo pairs using TruthseekerJ, available from the authors.[5,6] At the time of grading, human graders were masked from each others' results. They were also masked to the SD-OCT images and the clinical information associated with the photographs. A *reference standard* grading with a unique class (cup, rim, and background) assigned to each pixel was then created by combining the grading by each expert grader in a majority-win manner: Each pixel was assigned the class that received the majority of votes (e.g., if two graders voted a pixel to be rim and one grader to be cup, the pixel was designated rim). In the case of a draw, the pixel was assigned the background class. This reference standard was used for training and evaluation of the segmentation algorithm, as in our previous work (Fig. 1).

Preprocessing of SD-OCT Volumes

We preprocessed the raw OCT volume by detecting three surfaces, using a fast, three-dimensional multiscale layer segmentation algorithm that uses a graph search approach.[17–20] When these three surfaces are segmented, the approximate size, shape, and position of the ONH region are not yet known, and so a large region that is expected to include the ONH (based on the assumption that this is an ONH centered scan) is excluded from surface detection. Surface 1 corresponds to the internal limiting membrane (ILM), surface 2 lies between the inner and outer segments of the photoreceptors, and surface 3 is the outer boundary of the retinal pigment epithelium (RPE; Fig. 2).

Because patients are almost never imaged precisely through the optical axis and center of the pupil, skewness and curvedness are present in the OCT volume. To correct for this skew, we fit surface 3 to a thin-plate spline, excluding the area of the ONH (where no surface 3 exists) as approximated earlier, interpolate this spline through the ONH area, and then reconstruct the entire OCT volume to make surface 3 a plane—a process called flattening. The flattening step thus reduces the geometric distortion of the optic nerve head, making the subsequent classification step more robust.[17] We have published this robust, three-dimensional flattening technique in more detail elsewhere20 (Fig. 3).

Propagation of the Stereo Color Image–Based Reference Standard to OCT Volume

To train and evaluate the classification algorithm, we must know the reference standard class (cup, rim, or background) for each voxel on surface 1 (i.e., at the level of the visible retina). The surface voxels are also called the en face or *projection* image of the OCT volume.[21] In other words, the reference standard, as determined in the previous section, must be translated from pixels in the stereo color photograph to voxels in the SD-OCT image, by co-localization of the color image of the disc to the OCT volume. Retinal vessels are the anatomic structures with high contrast in both color images and OCT volume and are therefore suitable landmarks for co-localization. Segmenting the vessels in the color image of the optic disc, as well as the vessels in the OCT volume, superposition of the reference standard (which has the same coordinate system as the color image of the optic disc on which it was created) to the OCT volume, and assignment of the cup/rim/background label on the optic nerve head surface to the voxels below it, results in the expert assigned cup/rim/background label for each voxel, as we have described in more detail elsewhere (Fig. 4) (Lee S, et al. *IOVS* 2008;49:ARVO E-Abstract 1833).[19,22–24]

Classification of SD-OCT Volumes from Voxel Column Features

By defining voxel columns extending vertically from the surface of the retina or optic nerve head (surface 1) to the level of the RPE or its extension through the optic nerve head (surface 3), we were able to calculate 10 voxel column features as follows:

- Features 1, 2: distances in *x, y* dimension from the lowest point of surface 1 (approximately corresponding to the distance to the deepest point in the cup excavation).
- Feature 3: the distance between surface 1 and the thin plate spline fitted to surface 3, approximately corresponding to the local thickness of the retina between the ILM and the RPE, or, or approximately the corresponding level in the optic nerve canal, in the optic nerve head region.
- Feature 4: the average intensity in the voxel column between the ILM and surface 2, the boundary between inner and outer segments of the photoreceptors.
- Features 5–9: the average intensity in the current voxel column and the four directly neighboring columns next to it, between the ILM and surface 2.

- Feature 10: average voxel intensity between surfaces 2 and 3.

These voxel columns traverse the entire volume and are thus not true 3-D structures, in other words, they have eight neighbors and the four direct (closest) neighbors are used for features 5 to 9. All training feature values were dimensionless and normalized to unit variance and 0 mean and these same values were used to normalize the testing features derived from test images. This feature vector was used for each voxel column and was then classified using a *k*-NN classifier, with the number of neighbors, *k*, set to 7.[6] Preliminary experiments showed choosing $k = 7$ performed well, but the overall performance of the algorithm did not change much when *k* was varied. We used the approximate nearest neighbor classifier developed by Arya et al.,[25] as in our previous work. Feature selection was not performed in this preliminary study. The appearance of the *k*-NN segmentation is pixelated, because it operates on voxel columns independently.[6] To smooth the appearance of the *k*-NN segmentation result, we used a nine *k*-NN classifier, which finds the most frequent label of nine *k*-NN classifications in a 3 × 3 voxel column area, an approach described in detail in a technical paper.[19]

Testing the Classification Algorithm

The algorithm in this study is a so-called supervised algorithm, requiring a training phase, during which correctly labeled (from the reference standard) voxel columns are required, and a testing phase of the performance on SD-OCT volumes that were excluded from the training set. To have an unbiased performance metric and given the limited number of eyes available for testing, we used a so-called jackknife or leave-four-out approach. We repeated the experiment nine times, each time selecting 4 unique SD-OCT volumes from the 34 SD-OCT volumes of the left eye, to serve as the test set for that experiment, and using the remaining 30 SD-OCT volumes of the left eye as the training set. Thus, no SD-OCT volume in a training set ever occurred in a test in that experiment. For training, the reference standard from three glaucoma specialists was used as the distance of the disc, and cup boundaries in surface voxels (pixels) was used as the reference standard (Fig. 4).

Data Analysis

As in our Previous study, the Performance of the algorithm was evaluated by using two metrics. The first one was the accuracy of all voxels on the surface of the segmented OCT scan (i.e., the number of surface voxels that had the same label as the reference standard) for both rim and cup. The second measure was the correlation of the linear cup-to-disc ratio of the segmented ONH volume to the cup-to-disc ratio of the reference standard. The linear cup-to-disc ratio was then computed for each graded image as a square root of area cup-to-disc ratio:

$$cd_{r,\text{linear}} = \sqrt{\frac{n_{c,P}}{n_{r,P} + n_{c,P}}}$$

where $n_{r,P}$ is the number of surface voxels in each image that the algorithm estimated were rim, and $n_{c,P}$ is the number of surface voxels that were estimated to be cup.[26] This linear c/d ratio is a succinct metric that does not require estimating sectors on the disc and summarizes the c/d of all meridians including the vertical and horizontal c/d in a single number.

In addition to these objective metrics, it is preferable that preliminary studies that compare an algorithm to human experts show face validity. Thus, we selected a random sample of every third patient, 12 patients overall, and created 3-D surface renderings of the SD-OCT volume with the algorithm-determined cup and disc mapped in color, as well as SD-OCT projection images with the cup and rim mapped in color.

RESULTS

The SD-OCT volumes of 34 left eyes of 34 consecutive patients were included to test the algorithm. The age of these patients was 70 ± 15 years (mean ± SD), and 54% were women. Six had suspected glaucoma, 23 open-angle glaucoma, 2 angle-closure glaucoma, and 3 combined-mechanism glaucoma.

Three glaucoma specialists performed planimetry on the stereo color photographs, and this resulted in 34 segmented ONH SD-OCT volumes, with each *x*, *y* surface voxel labeled as either cup, rim, or background, for data analysis.

The average rim accuracy of the algorithm (i.e., the number of rim surface voxels the algorithm correctly assigned as rim in the reference standard was 80% ± 18%), and the average cup accuracy was 59% ± 13%. The correlation of the linear c/d of the algorithm to experts 1, 2, and 3 was respectively 0.90, 0.87, and 0.93 respectively, and to the reference standard (i.e., the combination of experts 1, 2, and 3) was 0.92. Figure 5 shows a scatterplot of the correspondence between a randomly chosen expert, and the algorithm and the other two experts. The correlations of the linear c/d of experts 1 to 2, 1 to 3, and 2 to 3, were 0.89, 0.93, and 0.88, respectively. Figure 6 is a visual illustration of the algorithm's performance versus the experts shown in two- and three dimensions, intended to help judge face validity. It can be seen that the expert cup and rim planimetry (shown on the OCT projection image), corresponds quite closely to the algorithm cup and rim planimetry on this random sample from all 34 optic nerve head segmentations. Subgroup analysis was not performed, given the small sample size.

DISCUSSION

The results of this preliminary study show that the performance of an automated algorithm for determination of the cup and rim from close-to-isotropic SD-OCT images correlates highly with that of planimetry by glaucoma experts on the same eye.

To our knowledge, this is the first such algorithm. If these preliminary results can be confirmed in a larger study, such algorithms, to automatically segment cup and rim from SD-OCT, have the potential to replace or substitute for time-consuming expert planimetry, which also suffers from interobserver variability.[5] Because evaluation of the optic disc and planimetry are an important part of the evaluation of patients with glaucoma, such algorithms may offer improved management of patients with glaucoma. In this preliminary study, we have not compared the performance of this, SD-OCT-based, algorithm to the performance of our previously published stereo color photograph–based algorithm.[6] We are currently studying the performance of an improved version of the stereo color photograph algorithm. The lower accuracy of the algorithm on cup than on rim is to be expected, as glaucoma specialists base their rim planimetry on relatively easy to define image structures, while the cup planimetry is based on more subjective assessment of a boundary on a gradual, relatively featureless, slope. The algorithm is trained on the planimetry from color stereo photos. Because the algorithm is trained for rim voxels on a less variable rim margin human expert reference standard, as well as a more variable cup boundary reference standard, whereas the rim voxels only depend on the more variable cup boundary reference standard, the rim area is less variable than the cup area.

There are several shortcomings in this study. First, the number of subjects is too small to unequivocally determine the performance relative to glaucoma experts. Second, this algorithm currently works on close-to-isotropic SD-OCT volumes. This study was performed on SD-OCT devices from only a single manufacturer, but we obtained subjectively similar results on a second close-to-isotropic SD-OCT device (Topcon, Paramus, NJ). The performance can be expected to be lower on more anisotropic OCT volumes, where the distance between B-scans is much larger. Third, although c/d ratio and expert planimetry are important components of

the evaluation of patients with glaucoma, other features of the optic disc, visible through biometry and stereo color photography, such as color changes, are lost. The additional value, if any, of such features remains to be determined, especially for their relevance to the measurement of progression of glaucoma. Fourth, because we expect the main application of this algorithm to be in glaucoma staging, rather than differentiating normal from glaucoma cases, we have not tested the algorithm's performance on normal eyes. Some of the patients had suspected glaucoma with a small c/d, and the algorithm did not show bias in these cases.

Finally, we essentially compressed the information contained in the ONH OCT volume into a single number, the c/d ratio. The cup and rim are attractive because they are easily understood by clinicians and allow comparisons to other studies. It is possible, and in fact likely, that other parameters of the ONH, determined from SD-OCT volumes, correlate at least as well or better than the cup and rim to glaucoma diagnosis and progression. For example, the work by Burgoyne and Downs[13] shows that features of the lamina cribrosa are important parameters of glaucoma progression. Because we detect the rim and cup, we could also have compressed the ONH information into a different number—for example, the rim surface. We have focused in this study on the c/d ratio because it is a measure that is in widespread clinical use, and most clinicians are familiar with its limitations, more so than with those of newer measures. Thus, validation of this algorithm on a larger cross-sectional glaucoma sample as well as the normal control is warranted, to determine unequivocally its correspondence to glaucoma experts. More important, longitudinal evaluation of a sample of persons with glaucoma, will allow its potential, if any, to detect glaucoma progression to be determined.

In summary, in this preliminary study, we developed a novel algorithm to determine the cup and rim in close-to-isotropic SD-OCT images of the ONH and showed that its performance for determination of the cup and rim from these SD-OCT images is essentially equal to that of planimetry performed by glaucoma experts on the same eye.

Acknowledgments

Supported by Carl Zeiss Meditec, Inc. (MDA, MKG, MS, KL), National Institutes of Health Grant EY017066 (MDA, WLMA), Research to Prevent Blindness (MDA, YHK), U. S. Department of Agriculture; University of Iowa (MDA); the Netherlands Organization for Health Related Research (MDA, MN); and the Marlene S. and Leonard A. Hadley Glaucoma Research Fund (MDA, YHK). WLMA is a Lew R. Wasserman award recipient from RPB.

References

1. Tielsch JM, Sommer A, Katz J, Royall RM, Quigley HA, Javitt J. Racial variations in the prevalence of primary open-angle glaucoma: The Baltimore Eye Survey. JAMA 1991;266(3):369–374. [PubMed: 2056646]
2. Heijl A, Leske MC, Bengtsson B, Hyman L, Bengtsson B, Hussein M. Reduction of intraocular pressure and glaucoma progression: results from the Early Manifest Glaucoma Trial. Arch Ophthalmol 2002;120(10):1268–1279. [PubMed: 12365904]
3. Greaney MJ, Hoffman DC, Garway-Heath DF, Nakla M, Coleman AL, Caprioli J. Comparison of optic nerve imaging methods to distinguish normal eyes from those with glaucoma. Invest Ophthalmol Vis Sci 2002;43(1):140–145. [PubMed: 11773024]
4. Tielsch JM, Katz J, Quigley HA, Miller NR, Sommer A. Intraobserver and interobserver agreement in measurement of optic disc characteristics. Ophthalmology 1988;95(3):350–356. [PubMed: 3174002]
5. Kwon Y, Adix M, Zimmerman MB, et al. Variance due to observer, repeat imaging, and fundus camera type on cup-to-disc ratio estimates by stereo planimetry. J Glaucoma 2009;18(4):305–310. [PubMed: 19365196]
6. Abramoff MD, Alward WL, Greenlee EC, et al. Automated segmentation of the optic nerve head from stereo color photographs using physiologically plausible feature detectors. Invest Ophthalmol Vis Sci 2007;48:1665–1673. [PubMed: 17389498]

7. Xu J, Ishikawa H, Wollstein G, et al. Automated assessment of the optic nerve head on stereo disc photographs. Invest Ophthalmol Vis Sci 2008;49(6):2512–2517. [PubMed: 18326698]
8. Merickel, JMB.; Abramoff, MD.; Sonka, M.; Wu, X., editors. Medical Imaging 2007: Image Processing. San Diego, CA: SPIE; 2007. Segmentation of the optic nerve head combining pixel classification and graph search.
9. Merickel, JMB.; Wu, X.; Sonka, M.; Abramoff, M., editors. Medical Imaging 2006: Physiology, Function, and Structure from Medical Images. San Diego, CA: SPIE; 2006. Optimal segmentation of the optic nerve head from stereo retinal images.
10. Hee MR, Puliafito CA, Wong C, et al. Quantitative assessment of macular edema with optical coherence tomography. Arch Ophthalmol 1995;113(8):1019–1029. [PubMed: 7639652]
11. Wojtkowski M, Bajraszewski T, Gorczynska I, et al. Ophthalmic imaging by spectral optical coherence tomography. Am J Ophthalmol 2004;138:412–419. [PubMed: 15364223]
12. Leon Ortega JE, Sakata LM, Kakati B, et al. Effect of glaucomatous damage on repeatability of confocal scanning laser ophthalmoscope, scanning laser polarimetry, and optical coherence tomography. Invest Ophthalmol Vis Sci 2007;48(3):1156–1163. [PubMed: 17325159]
13. Burgoyne CF, Downs JC. Premise and prediction-how optic nerve head biomechanics underlies the susceptibility and clinical behavior of the aged optic nerve head. J Glaucoma 2008;17(4):318–328. [PubMed: 18552618]
14. Strouthidis NG, Yang H, Fortune B, Downs JC, Burgoyne CF. Detection of the optic nerve head neural canal opening within three-dimensional histomorphometric and spectral domain optical coherence tomography data sets. Invest Ophthalmol Vis Sci 2009;50(1):214–223. [PubMed: 18689697]
15. Yang H, Downs JC, Burgoyne CF. Physiologic Inter-eye Differences in monkey optic nerve head architecture and their relation to changes in early experimental glaucoma. Invest Ophthalmol Vis Sci 2009;50(1):224–234. [PubMed: 18775866]
16. Niemeijer, M.; Van Ginneken, B.; Abramoff, MD. Automated localization of the optic disc and fovea. 30th Annual International IEEE EMBS Conference. 2008; IEEE; New York. 2008. p. 3538-3541.
17. Haeker, M.; Abramoff, MD.; Wu, X.; Kardon, R.; Sonka, M. Use of varying constraints in optimal 3-D graph search for segmentation of macular optical coherence tomography images; Med Image Comput Comput Assist Interv Int Conf Med Image Comput Comput Assist Interv; 2007. p. 244-251.
18. Haeker M, Abràmoff MD, Kardon R, Sonka M. Segmentation of the surfaces of the retinal layer from OCT Images. Lecture Notes Comp Sci 2006;4190:800–807.
19. Lee KN, Garvin MK, Kwon YH, Sonka M, Abramoff MD. 3-D segmentation of the rim and cup in spectral-domain optical coherence tomography volumes of the optic nerve head. Proc SPIE 2009. In press.
20. Garvin MK, Abramoff MD, Wu X, Russell SR, Burns TK, Sonka M. Automated 3-D intraretinal layer segmentation of macular spectral-domain optical coherence tomography images. IEEE Trans Med Imaging 2009;28(9):1436–1447. [PubMed: 19278927]
21. Van Dijk HW, Kok PH, Garvin M, et al. Selective loss of inner retinal layer thickness in type 1 diabetic patients with minimal diabetic retinopathy. Invest Ophthalmol Vis Sci 2009;50(7):3404–3409. [PubMed: 19151397]
22. Niemeijer M, Staal JS, van Ginneken B, Loog M, Abramoff MD. Comparative study of retinal vessel segmentation on a new publicly available database. Proc SPIE 2004:5370–5379.
23. Niemeijer, M.; Garvin, MK.; van Ginneken, B.; Sonka, M.; Abramoff, MD., editors. Medical Imaging 2008: Image Processing. San Diego, CA: SPIE; 2008. Vessel segmentation in 3D spectral OCT scans of the retina.
24. Lee, S.; Abramoff, MD.; Reinhardt, JM. Validation of retinal image registration algorithms by a projective imaging distortion model; Conf Proc IEEE Eng Med Biol Soc; 2007. p. 6472-6475.
25. Arya S, Mount D, Netanyahu N, Silverman R, Wu A. An optimal algorithm for approximate nearest neighbor searching in fixed dimensions. J ACM 1998;45(6):891–923.
26. Shuttleworth GN, Khong CH, Diamond JP. A new digital optic disc stereo camera: intraobserver and interobserver repeatability of optic disc measurements. Br J Ophthalmol 2000;84(4):403–407. [PubMed: 10729299]

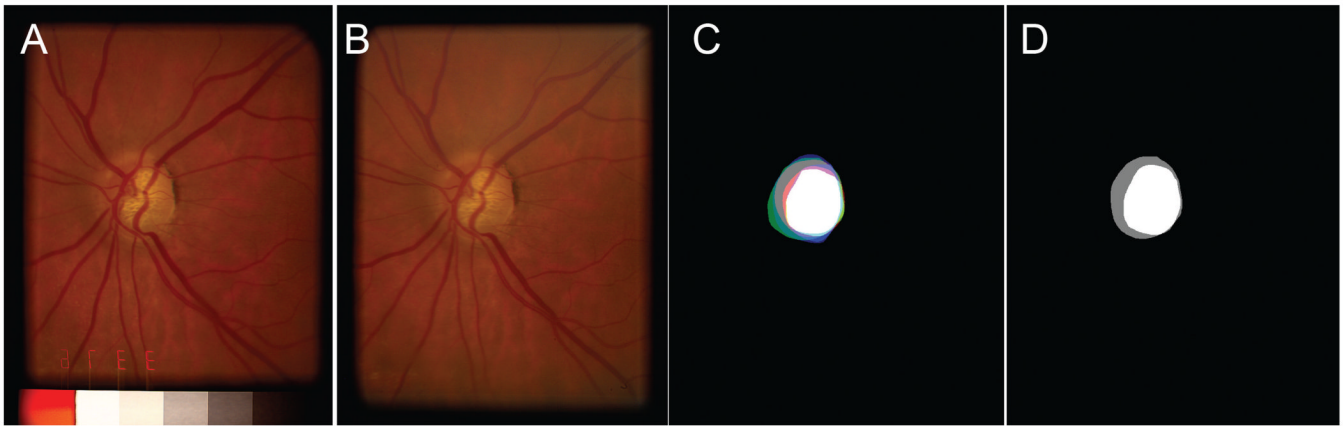

FIGURE 1.

(**A**, **B**) Left and right image of a stereo pair of an optic disc, the original captured image was cropped and separated. The left and right stereo images can be fused by holding the page at about 30 cm (12 in.) from the eye and gazing into infinity. (**C**) Planimetry by three glaucoma specialists superimposed, to show how the reference standard in (**D**) is created. It shows the cup and rim of each expert in *bright red*, *green*, and *blue* (rim), respectively, *pale red*, *green*, and *blue* (cup). Thus, where all three experts indicated cup, *white* is shown, and where all three experts indicated rim, *gray* is shown. (**D**) Reference standard developed from the planimetries shown in (**C**).

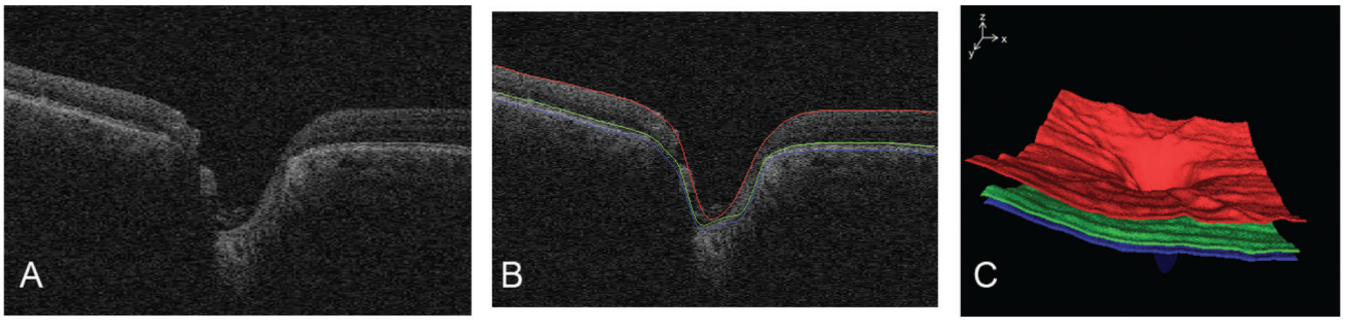

FIGURE 2.

Layer segmentation before flattening. (**A**) Single slice of SD-OCT scan of optic nerve head of the same patient and the same eye as in Figure 1. (**B**) Three surfaces segmented by using fast layer segmentation. (**C**) Surface rendering of these three surfaces.

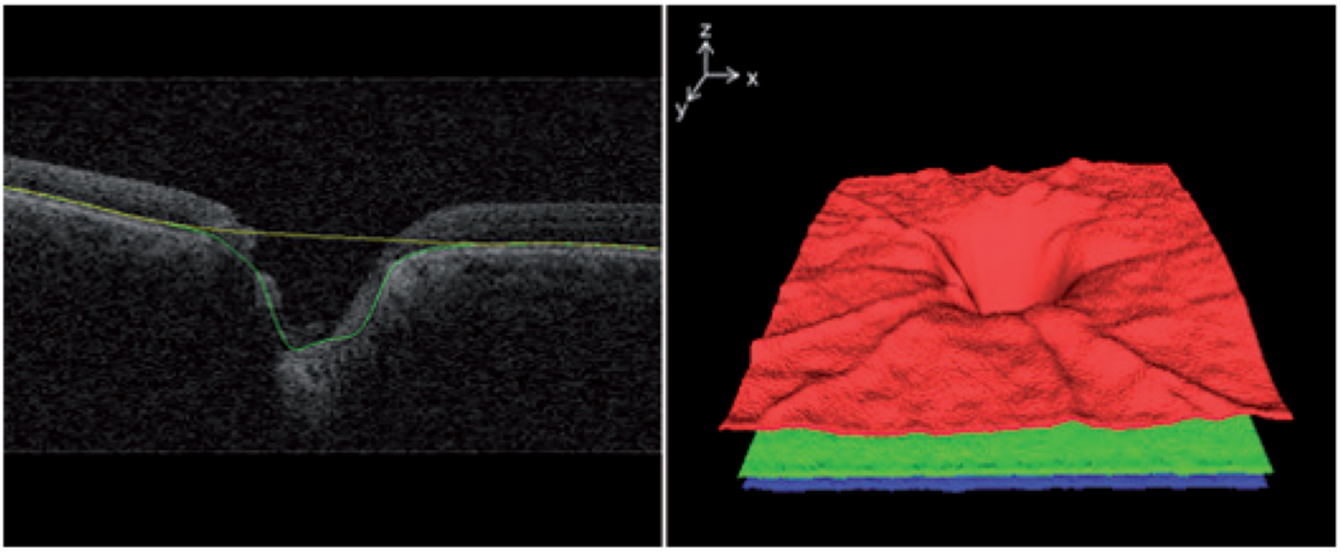

FIGURE 3.

Volume-flattening step. *Left*: after three surfaces have been detected, a 3-D thin plate spline is fitted to the surface, except through the area of the ONH, where this spline is extrapolated. *Right*: the entire volume is then reconstructed, also in 3-D, based on this spline fitted to surface 3.

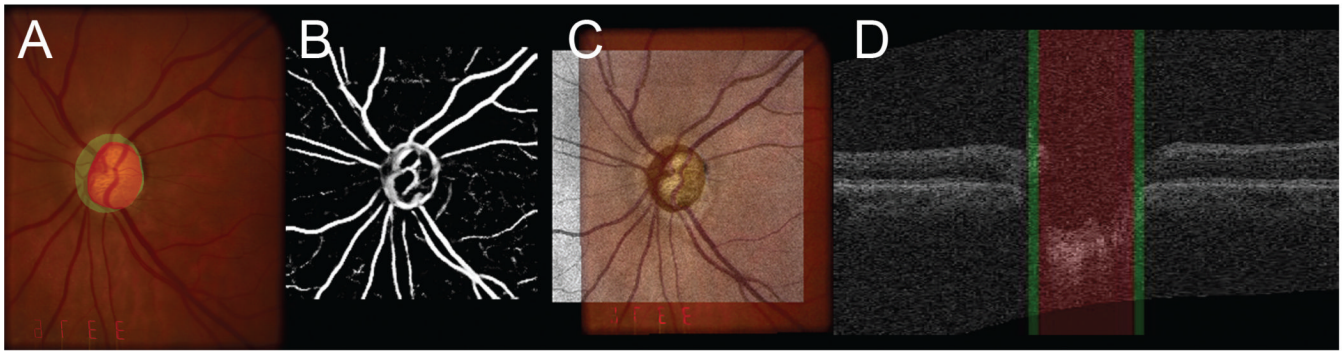

FIGURE 4.

Propagation of the reference standard from stereo color image–based planimetry to SD-OCT volume. (**A**) Left stereo color fundus image with superimposed reference standard (*reddish* cup, *greenish* rim). (**B**) Vessel segmentation in a surface projection of an SD-OCT image. (**C**) Co-localization of an SD-OCT projection image and left stereo color fundus image. (**D**) Propagation of cup (*reddish*) and rim (*greenish*) voxel columns from the reference standard in a stereo color fundus image into an SD-OCT image (single vertical slice shown) based on co-localization in (**C**).

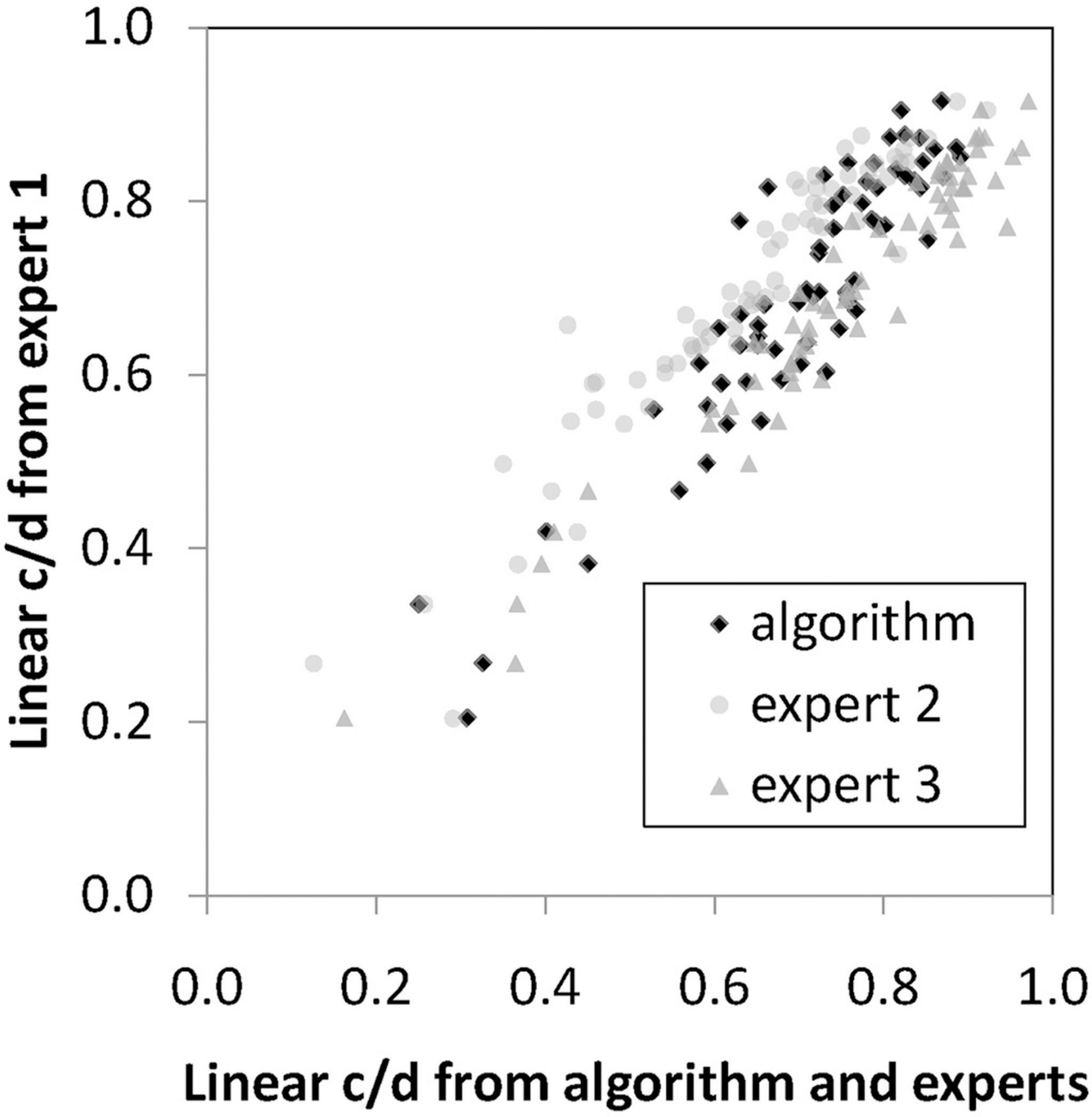

FIGURE 5.
The correlation of the algorithm-determined linear c/d with that of any glaucoma specialist was not inferior to the correlation of any glaucoma specialist to any other glaucoma specialist. Scatterplot of linear c/d of the algorithms presented in this paper and of glaucoma specialist 2 and glaucoma specialist 3, when the algorithm was trained on the reference standard for the training set only cup and disc segmentation only.

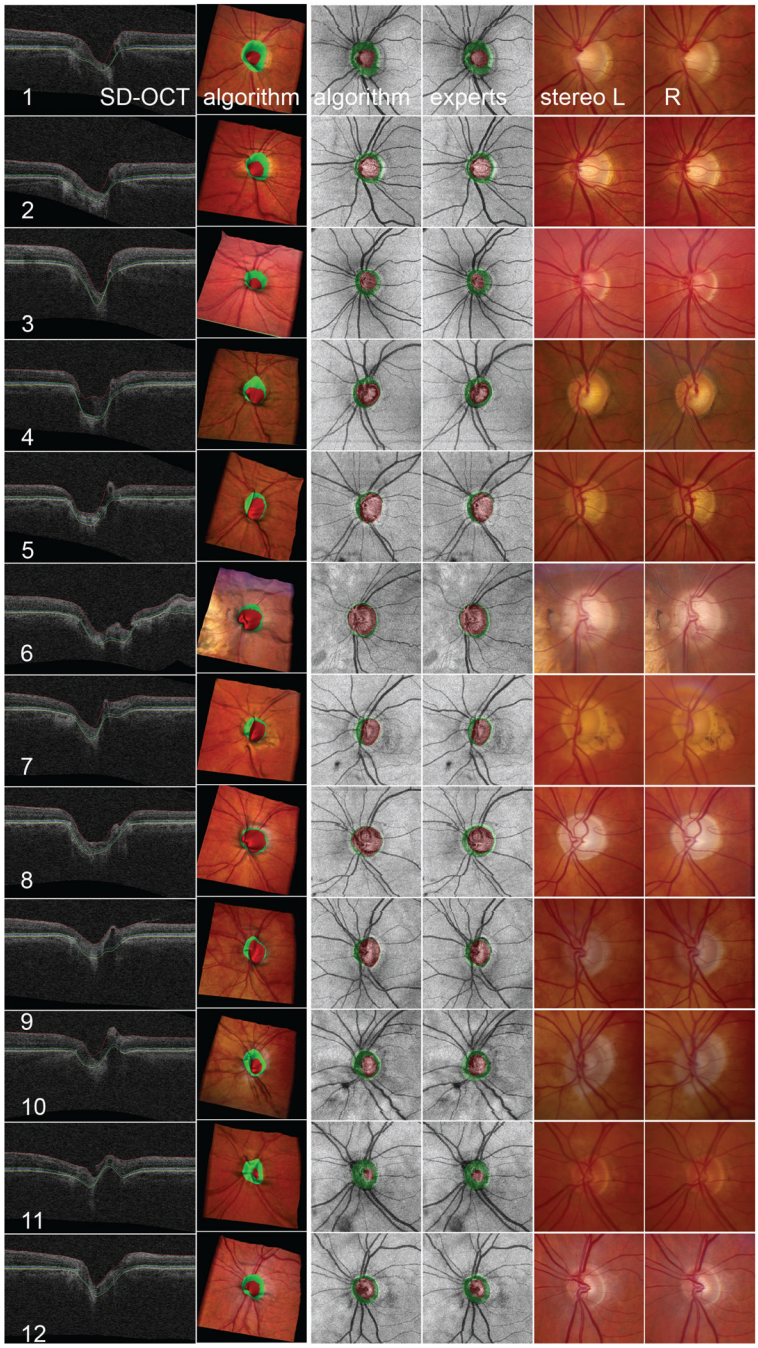

FIGURE 6.

Visualization of the performance of automated segmentation of an optic nerve head (ONH) from SD-OCT for 12 of 34 randomly selected eyes, compared with the performance of three glaucoma specialists. Top to bottom rows 1–12: 12 patients, left eye. *Left* to *right*: SD-OCT: central slice 100/200 of the SD-OCT volume through the center of the disc, oriented from nasal (*left*) to temporal (*right*), with three detected surfaces indicated; algorithm: visualization of the detected cup (*reddish*) and rim (*greenish*) on a 3-D surface rendering of the ONH wrapped with color fundus photograph (the shape of the surface derived from the OCT and the color of the surface derived from the co-registered color image) to show the three-dimensional relationship of the cup and rim; algorithm: detected cup and rim on SD-OCT projection image;

experts: propagation of the reference standard created by three glaucoma specialists from stereo color photos onto SD-OCT projection image; stereo L and R: left and right color stereo photos that experts used to obtain reference standard.